https://doi.org/10.5194/egusphere-2026-3873
Preprint. Discussion started: 14 August 2026

Local Controls on the Development of Percolation Features After a Rain-on-Snow Event in a Southern Taiga Snowpack

Anton Komarov[1,2], Julienne Stroeve[1,2,3]

[1] Alfred-Wegener-Institut Helmholtz-Zentrum für Polar- und Meeresforschung, Bremerhaven, Germany

[2] Centre of Earth Observation Science (CEOS), University of Manitoba, Winnipeg, Canada

[3] Alfred Wegener Institute (AWI), Institute of Environmental Physics (IUP), University of Bremen, Germany

Correspondence to: Anton Komarov (anton.komarov@awi.de)

Abstract. Rain-on-snow (ROS) events can rapidly introduce liquid water into cold snowpacks. However, direct field observations of preferential-flow structure development under such conditions remain limited. In this study, we document the formation of percolation columns and linear flow pathways after a ROS event in a cold, predominantly fine-grained snowpack in the southern taiga. We combine meteorological observations, snow-pit measurements, stratigraphic descriptions, density and snow-water-equivalent (SWE) measurements, and low-cost photogrammetric mapping to examine how local surface conditions influenced the spatial organization of preferential flow.

The same ROS event produced contrasting flow structures over short distances. In the floodplain meadow, percolation features developed mainly in inter-tussock depressions and formed relatively large funnels with the highest areal coverage. In the more homogeneous field site, features were more numerous but smaller, while in the birch forest they were sparse and clustered, mainly in canopy gaps. On the slope (~25°), liquid water was routed into elongated, downslope flow pathways rather than discrete vertical columns. At the meadow and field sites, snow within percolation columns was denser and stored more SWE than the surrounding snow occupying the same volume, indicating localized water accumulation and refreezing.

These results show that rain-induced infiltration in cold snowpacks can be reorganized at sub-meter scales by microtopography, vegetation, slope, and snow stratigraphy. Percolation columns and associated ice structures therefore represent important small-scale heterogeneities that can affect meltwater storage, refreezing, drainage pathways, causing challenges in snowpack modelling, and the interpretation of microwave remote-sensing signals.

1. Introduction

Snow plays a crucial role in hydrology, climate, and ecosystem functioning by acting as a temporary reservoir that regulates the release of water to rivers, lakes, groundwater systems, and soils (e.g. Barnett et al., 2005; Zhang, 2005; Rixen et al., 2022). As an effective thermal insulator, snow controls ground temperatures and protect soils and vegetation from extreme winter cold (Formozov, 1990; Sturm, 1992; Pomeroy and Brun, 2021). However, changing weather conditions are altering these interactions. Climate warming is increasing the fraction of liquid precipitation, along with modifying the frequency, timing,

https://doi.org/10.5194/egusphere-2026-3873
Preprint. Discussion started: 14 August 2026

and intensity of rain-on-snow (ROS) events across snow-covered regions (e.g. Bintanja and Andry, 2017; Stroeve et al., 2022). Unlike gradual spring melt, ROS events can introduce substantial amounts of liquid water into the snowpack over short timescales, rapidly changing snowpack thermal and hydrological conditions (Putkonen and Roe, 2003; Würzer et al., 2016).

Initial snowpack inhomogeneity, including contrasts in grain size, density, stratigraphy, permeability, and capillary properties, strongly influences how liquid water moves through snow. Instead of wetting the snow matrix uniformly, water can concentrate in preferential vertical or lateral pathways, producing strong contrasts between wetted and comparatively dry parts of the snowpack (Colbeck, 1972; Hirashima et al., 2014; Leroux and Pomeroy, 2017). Fine-grained snow generally has stronger capillary retention than coarse-grained snow and may support more uniform wetting under some conditions, but the actual flow regime depends on water input rate, initial snow structure, and hydraulic contrasts between layers (Albert et al., 2000; Katsushima et al., 2013). Under ROS conditions, preferential flow may therefore develop even in cold, initially dry, or predominantly fine-grained snowpacks when liquid-water input exceeds local retention and transmission capacity, or where crusts, ice lenses, stratigraphic boundaries, and capillary barriers focus water movement and promote lateral redistribution, localized accumulation, and refreezing (Katsushima et al., 2009; Hirashima et al., 2017; Würzer et al., 2017; Moure et al., 2023; Yamaguchi et al., 2012; Lombardo et al., 2025).

In addition to internal snow structure, the spatial organization of percolation features can be influenced by surface and vegetation conditions. Microtopography and vegetation affect snow depth, density, layering, thermal gradients, and the location of depressions or inter-tussock hollows (Sturm and Holmgren, 1994; Komarov, 2021a; Komarov, 2021b; Komarov and Sturm, 2023). These localized variations determine where liquid water is retained, redirected, or funnelled into the snowpack, increasing its small-scale inhomogeneity. Although preferential-flow processes have been widely studied in melting snowpacks and laboratory experiments, direct field observations of their development in cold, fine-grained snow following natural ROS events remain limited (Hirashima et al., 2017; Webb et al., 2022; Madore et al., 2022).

The implications of percolation features extend beyond the assessment of the distribution of liquid water within the snowpack and their influence on water storage, drainage pathways, the timing of water release, and the spatial variability of snowpack properties. In some environments, such structures may also be relevant for wet-snow instability, glacier and firn hydrology, ground thermal conditions, and a wide range of ecosystem processes (Hock, 2005; Zhang, 2005; Rixen et al., 2022). Specifically, ice crusts or internal ice layers can limit access to vegetation, contributing to large-scale mortality in reindeer and caribou populations, with widespread impacts on ecosystems and local livelihoods (Bartsch et al., 2010; Forbes et al., 2016; Serreze et al., 2021). Their presence is also important for remote sensing because vertically and laterally heterogeneous wet or refrozen structures can modify signal propagation, backscatter, penetration depth (Colbeck, 1972; Hirashima et al., 2010; Donahue and Hammonds, 2022; Stroeve et al., 2022). They cause uncertainties in assessment and interpretation of snow wetness, snow water equivalent, and internal layering (Wiesmann and Mätzler, 1999; Montpetit et al., 2013; Zhu et al., 2021).

https://doi.org/10.5194/egusphere-2026-3873
Preprint. Discussion started: 14 August 2026

Spatially variable wetting and refreezing may also influence optical and near-infrared retrievals by altering surface grain size, crust formation, and reflectance (Nolin and Dozier, 2000; Kokhanovsky et al., 2018). Because percolation columns and associated ice structures often occur at sub-meter scales, they remain unresolved by snowpack models, introducing uncertainty into remote-sensing calibration, validation, and data assimilation (Liston, 2004; Komarov et al., 2018; Merkouriadi et al., 2021). Even high-resolution three-dimensional modelling frameworks underrepresent this type of small-scale heterogeneity in water infiltration and refreezing (Lehning et al., 2006; Mott et al., 2017).

Despite this relevance, the formation, morphology, and spatial distribution of percolation columns remain poorly studied under natural ROS conditions, particularly in cold, predominantly fine-grained snowpacks. Here, we present direct in situ observations of percolation-feature formation during a ROS event in the southern taiga. We analyze snow properties, stratigraphy, and meteorological forcing before and after the event, and examine how local surface conditions, vegetation, and slope influenced the spatial distribution and variability of preferential flow. The results provide field evidence of small-scale snowpack heterogeneity after ROS and have implications for snow hydrology, ecological interpretation, modelling, and remote-sensing applications under changing winter conditions.

In this study, terms are defined as follows: *percolation feature* serves as the general term for surface and internal expressions of preferential flow; *percolation funnels* denote surface depressions marking initial water entry points; *percolation columns* refer to vertically oriented, internal structures formed by localized wetting and refreezing; and *linear drainage pathways* describe elongated preferential flow features tracking down-slope terrain gradients.

2. Materials and methods

The study site was located in the Southern Taiga within the Central European Plain, approximately 70 km northeast of Moscow outside the influence of the metropolitan urban heat island (Komarov et al., 2025). The region experiences relatively mild winters characterized by large variability in air temperature and precipitation, with alternating cold spells and thaws, and a high potential for ROS events as a result of shifts between anticyclonic and cyclonic conditions. Snow cover typically lasts for three to four months, but its depth and properties vary from year to year (Komarov et al., 2019; Komarov et al., 2021; Sokratov et al., 2024).

To investigate snowpack evolution and the formation of percolation columns during ROS events, we combined analysis of weather data from nearby meteorological stations with detailed in-situ snow measurements conducted at the field sites.

Meteorological data included air temperature, precipitation, wind speed and direction from three stations: Sergiev Posad (10 km northeast of the study site), Alexandrov (45 km northeast), and Pushkino (30 km southwest). Air temperature and wind data were available from all three stations, while precipitation data were recorded only at Pushkino. Each parameter was measured at 3-hour intervals, allowing us to track weather fluctuations and their influence on snow properties in detail.

https://doi.org/10.5194/egusphere-2026-3873
Preprint. Discussion started: 14 August 2026

Snow properties and stratigraphy were measured during November and December 2024 near Khotkovo (56° 14′ 56″ N, 37° 59′ 54″ E), within a watershed landscape at altitudes ranging from 190 to 210 m above sea level. Snow measurements were conducted at four sub-sites with distinct surface microtopography, vegetation, and slope conditions (Supplement 1):

1. *Meadow* (Main Site) – A grassy floodplain meadow featuring pronounced microtopography, with tussocks 10–25 cm in height and 30–50 cm in diameter. This site was surrounded by trees, which protected it from wind and limited snow redistribution.
2. *Field* – A watershed field with 1-3 cm microtopography and short, homogeneous grass vegetation (3–5 cm) that had been cut before winter.
3. *Forest* – A location under the birch canopy with microrelief similar to the field site.
4. *Slope* – A steep slope (~25°) with limited microtopography and homogeneous grass vegetation.

At the main site, weekly measurements were made after the first snowfall on November 23 and until the end of the ROS event on December 24. On December 23 and 24, detailed snow pits were excavated at each site. These observations captured both pre- and post-infiltration phases, documenting percolation features formation and the disruption of snow layers.
Snow depth, density, snow water equivalent (SWE), temperature, and stratigraphy were recorded within 100 cm wide snow pits. At the meadow and field sites, we also conducted detailed percolation column analysis, including assessments of their morphology, density, SWE, and contribution to the snow mass balance. Additionally, measurements were performed on a steep slope near the study area to examine linear drainage formation. Snow depth and layer thickness were measured at the center of each 10 cm segment of 100 cm pits (10 points in total), and mean values were calculated in each pit. Snow temperature was measured using a manual temperature probe at the center of each snow layer. Snow density was measured at least three times per layer at lateral positions of 20, 50, and 80 cm along the pit using a standard 100 cm³ density cutter. Stratigraphic descriptions followed the International Classification for Seasonal Snow on the Ground (Fierz et al., 2009) and included snow type and crystal size, layer hardness and thickness, density, and SWE. The bulk SWE was calculated using the equation:

$$SWE = \sum_{i=0}^{n}(H_i * \frac{\rho_i}{\rho_w})$$

where

H_i – snow layer thickness (mm)

ρ_i – density of snow in the layer (kg/m3)

ρ_w – density of water (1000 kg/m3)

To describe the physical and morphological characteristics of individual percolation columns, we carefully excavated each column by gently removing the surrounding snow with a shovel and a soft brush. Each column was then photographed, measured, and systematically disassembled into its structural components, such as icy crusts and the column body. The dimensions and weight of each component were recorded to calculate the snow water equivalent (SWE) stored within it. While

https://doi.org/10.5194/egusphere-2026-3873
Preprint. Discussion started: 14 August 2026

this method has some inherent limitations in accuracy, it provides a reasonable estimate of the proportion of SWE stored in ice structures and their overall contribution to the snowpack's mass balance.

To assess the spatial distribution of percolation features, we used photogrammetric images captured with Scaniverse, a free LiDAR and photogrammetry application. This was done before destructive snow measurements. We generated 360° photogrammetric images with a scanning radius of approximately 3 m. For the three flat sites, we measured the diameter and area of percolation funnels, their total and relative surface coverage, and the mean nearest-neighbor distance between mapped features. The slope site was analyzed separately because preferential flow there formed elongated linear pathways rather than discrete circular funnels; for this site, we measured flow-path length and orientation. The raw images downloaded from Scaniverse were processed and manually annotated in a graphical editor, and were then analyzed using Python libraries in a Jupyter Notebook (*link to Zenodo will be provided upon acceptance*).

To evaluate scan reliability, distances between selected percolation-column centers were measured both in the Scaniverse-derived images and in the field using a ruler. These paired measurements provided a simple check of spatial accuracy for the distance range most relevant to nearest-neighbour analysis. Finally, we used these measurements to assess how percolation columns affected the spatial variability of SWE within the snowpack.

3. Results

3.1 Weather conditions

Weather conditions during the study period (23 November - 24 December) were highly variable, alternating between cold spells and thaw periods. Air temperatures ranged from −18 °C to +2 °C, while wind speeds fluctuated between 0 and 5 m s^{-1} (Figs. 1 and 2). Snow accumulation occurred mainly during three major snowfall periods: 21 - 24 November, 7 - 9 December, and 14 - 17 December, together with several smaller snowfall events in late November and the second half of December. These weather fluctuations played a key role in the formation of snow layers.

The initial snowfall, which formed the base of the snowpack, occurred under mild, near-freezing conditions, resulting in a compact basal layer. As temperatures dropped, subsequent snowfalls accumulated on top of this base. Persistent cold conditions from 4 to 21 December prevented melt events, and therefore no melt–freeze crusts formed during this period. The coldest conditions occurred around 20 December, when daily mean air temperature reached approximately −14 °C and minimum temperatures dropped to −18 °C. These conditions caused temperature-gradient metamorphism and faceted-grain growth in the lower snow layers. However, on 18 December, winds of up to 5 m s^{-1} combined with ongoing snow accumulation resulted in the formation of a soft wind slab layer.

On 21 December, air temperatures reached 2 °C and rainfall resulted in liquid-water input into the snowpack (Fig. 1, 2). Field observations suggest that the first portions of rain froze on contact with the below-zero snow surface, forming a thin, low-permeability crust at the snow–air interface. Throughout the night and early morning, air temperatures remained near or slightly above freezing (0 to +1.5 °C), with 100% cloud cover and moderate winds (1 - 4 m s^{-1}) from the south-southwest to southwest.

https://doi.org/10.5194/egusphere-2026-3873
Preprint. Discussion started: 14 August 2026

As precipitation continued, the surface crust likely limited uniform vertical infiltration and promoted short-distance lateral redistribution of liquid water toward depressions and low-lying areas. In these locations, water pooled and entered the snowpack through weak points in the crust, producing localized percolation. Later in the day, air temperature dropped to −7 °C (Fig. 2), refreezing the wet pathways and preserving their structure for subsequent analysis.

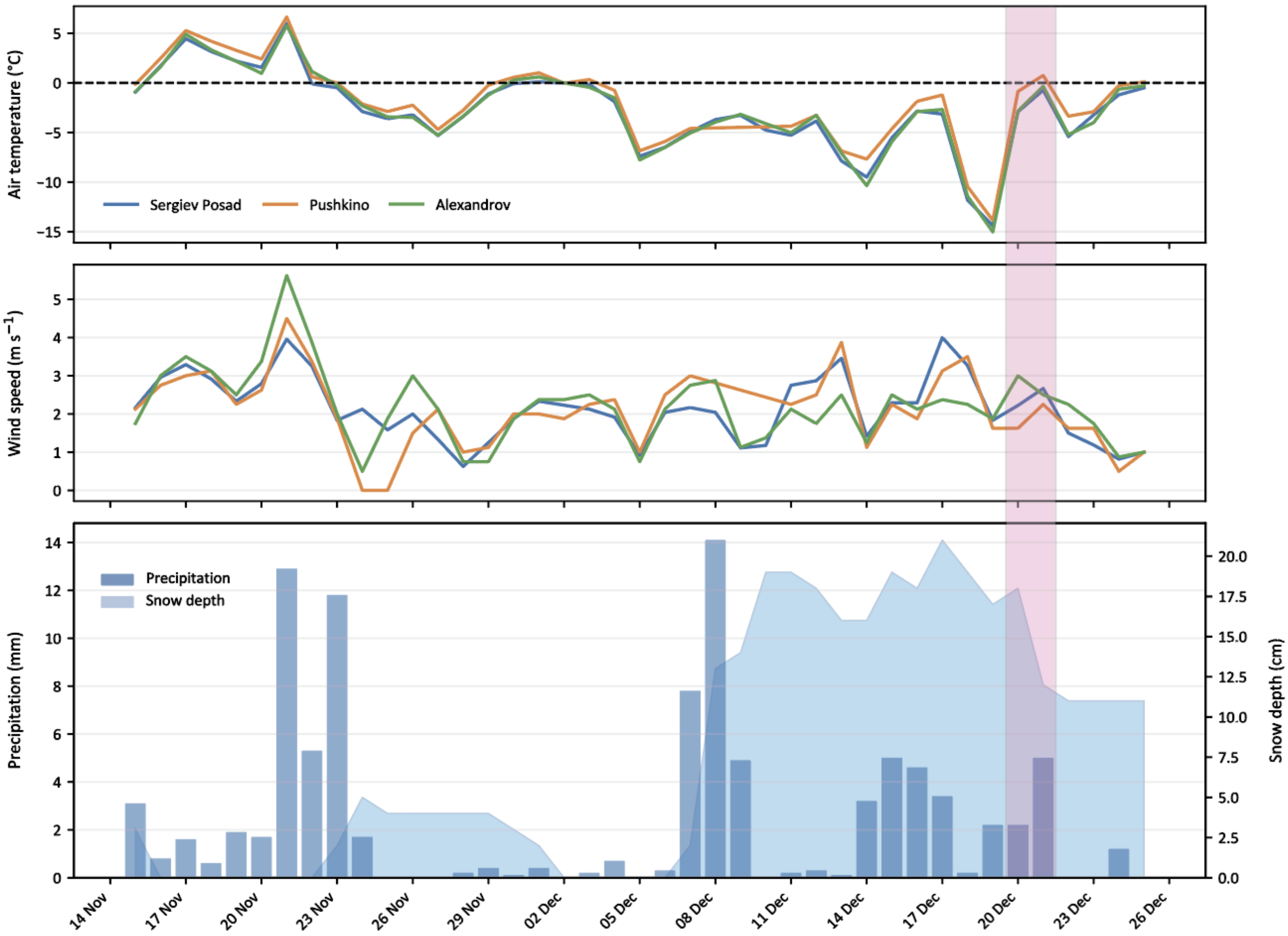

Fig. 1 Daily-averaged weather parameters (air temperature, wind speed, precipitation sum and snow depth) in November and December 2024 at the three weather stations located near the study sites. Snow depth and precipitation at the bottom plot were measured at Pushkino station. The pink strip indicates the ROS event.

https://doi.org/10.5194/egusphere-2026-3873
Preprint. Discussion started: 14 August 2026

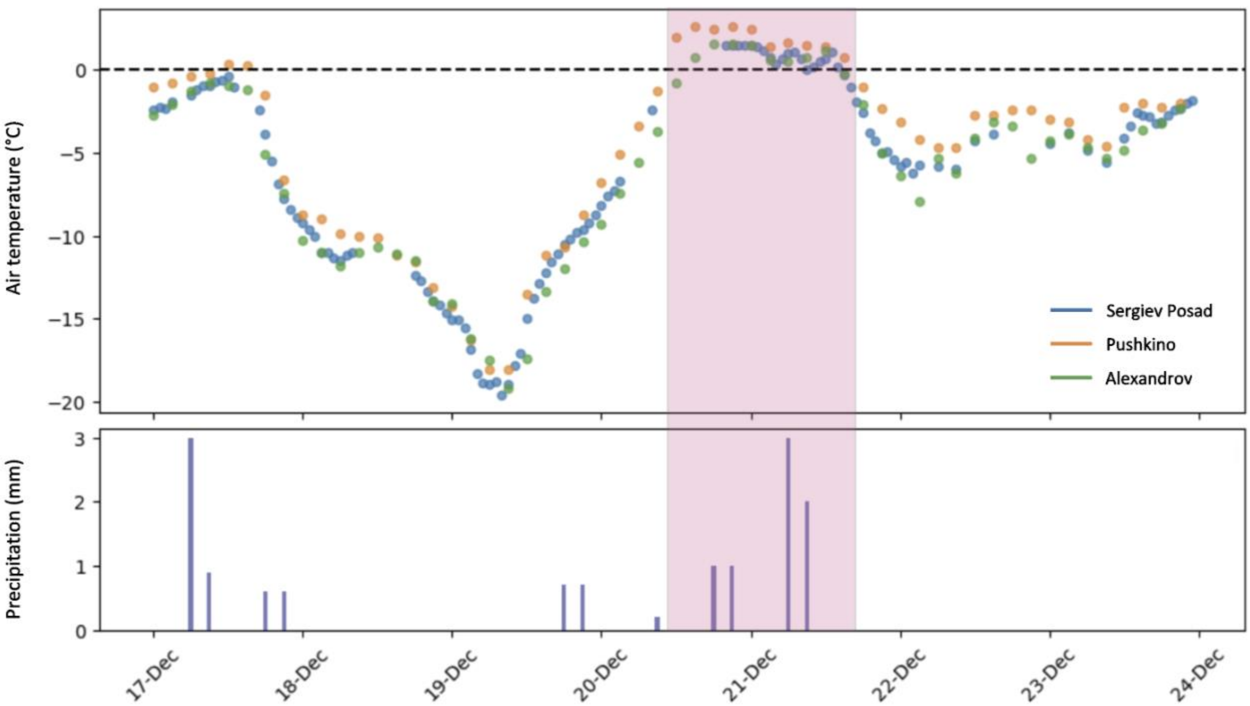

Fig. 2 Hourly-averaged weather parameters in 17 - 24 December 2024 at the three weather stations located near the study sites. The pink strip indicates the ROS event. The indicated precipitation was measured at the Pushkino station.

3.2 Snow Properties and Stratigraphy before and after ROS event

Snow depth, density, SWE, and stratigraphy were measured nearly every week from the onset of snow cover on November 23 until December 23. The first significant snowfall occurred on November 23, when approximately 3-5 cm of wet snow with a density of about 180 kg/m³ accumulated on unfrozen ground. By November 30, the snow had settled and partially melted due to above-freezing temperatures, forming a 2 - 3 cm layer of wet snow with a density of 200 - 220 kg/m³. This layer later froze, creating a melt-freeze layer at the snowpack base. However, this layer was observed only at the meadow site, while at the other sites it melted completely. On December 7, a major snowfall event deposited 10–12 cm of fresh snow with a density of 150–165 kg/m³, forming a two-layer stratigraphy at the meadow site and a single snow layer at the other three sites. By December 11, the snow depth increased to 18-20 cm at the field, slope and forest sites and 24 cm at the meadow site, as additional snowfall accumulated, forming a new layer of low-density (120–130 kg/m³) snow at the surface.

By 19 December, snow depth had increased to 24–28 cm and the snowpack consisted of four to five distinct layers. The uppermost layer was 5–7 cm thick and was composed of decomposed precipitation particles with low density (120–130 kg m⁻³). Below this, a 7–10 cm thick layer of denser wind-packed rounded grains had developed (200 kg m⁻³), followed by a nearly 1 cm thick decomposed crust or crust-like layer (280–300 kg m⁻³). Beneath this layer, faceted crystals and melt–freeze

https://doi.org/10.5194/egusphere-2026-3873
Preprint. Discussion started: 14 August 2026

clusters were observed (220 kg m⁻³), transitioning into a harder basal melt–freeze crust at the meadow site (approximately 250 kg m⁻³). Thus, the sites had broadly similar, but not identical, snow stratigraphy before the ROS event.

By 23 December, snow depth had decreased and a thin hard ice crust had developed at all sites, while the overall snow stratigraphy remained broadly similar (Fig. 3). However, pronounced percolation features developed at the study sites and differed clearly in size, volume, morphology, and spatial distribution.

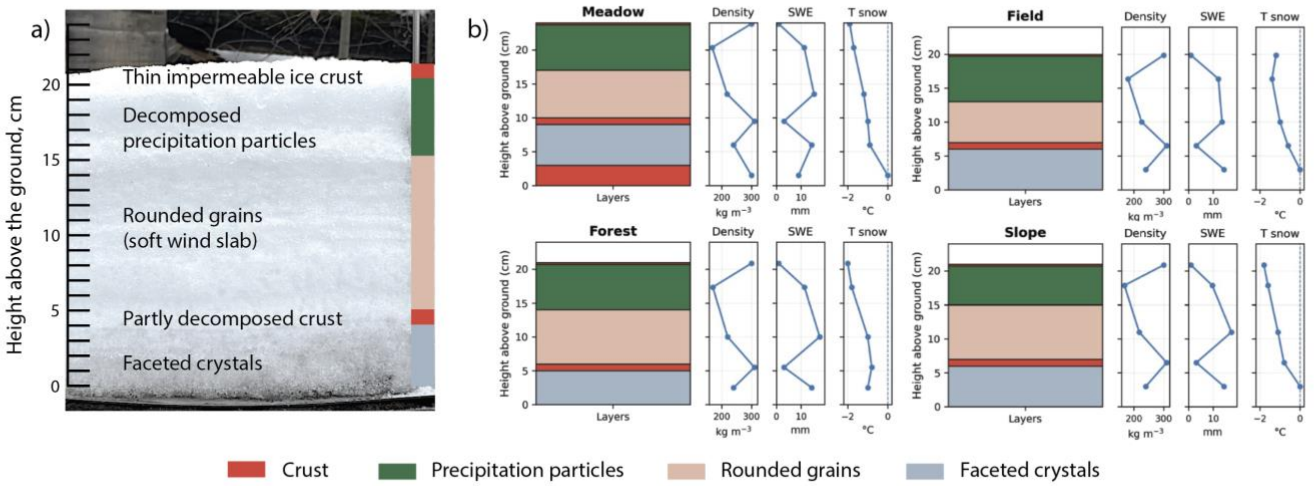

Fig. 3 Snow stratigraphy and properties at the field site (a) and all the four study sites (b) on December 23, two days after the ROS event. While the overall snow stratigraphy and snow properties were similar at all sites, total snow thickness was slightly larger at the meadow site mostly due to presence of melt-freeze layer at the bottom.

3.3 Spatial distribution of percolation features

The morphological expression of preferential flow during the ROS event is governed by terrain geometry, diverging between the flat and sloping sub-site. Will infiltration at the three flat sites resulted in vertically oriented percolation columns topped by surface funnels, flow at the slope site was redirected laterally, forming elongated linear drainage pathways. Despite the three flat sites sharing a similar vertical flow regime, there was pronounced microscale variations in funnel density, dimensions and spatial clustering, driven by localized differences in ground microtopography and vegetation cover (Figs. 4 and 5).

To quantify these structural differences across the flat terrain, in situ data and photogrammetric images acquired with Scaniverse were analyzed to assess the diameter and area of percolation funnels, their surface expression, as well as the mean nearest-neighbor distance between them. The slope site was analyzed separately using the length and orientation of linear flow paths.

https://doi.org/10.5194/egusphere-2026-3873
Preprint. Discussion started: 14 August 2026

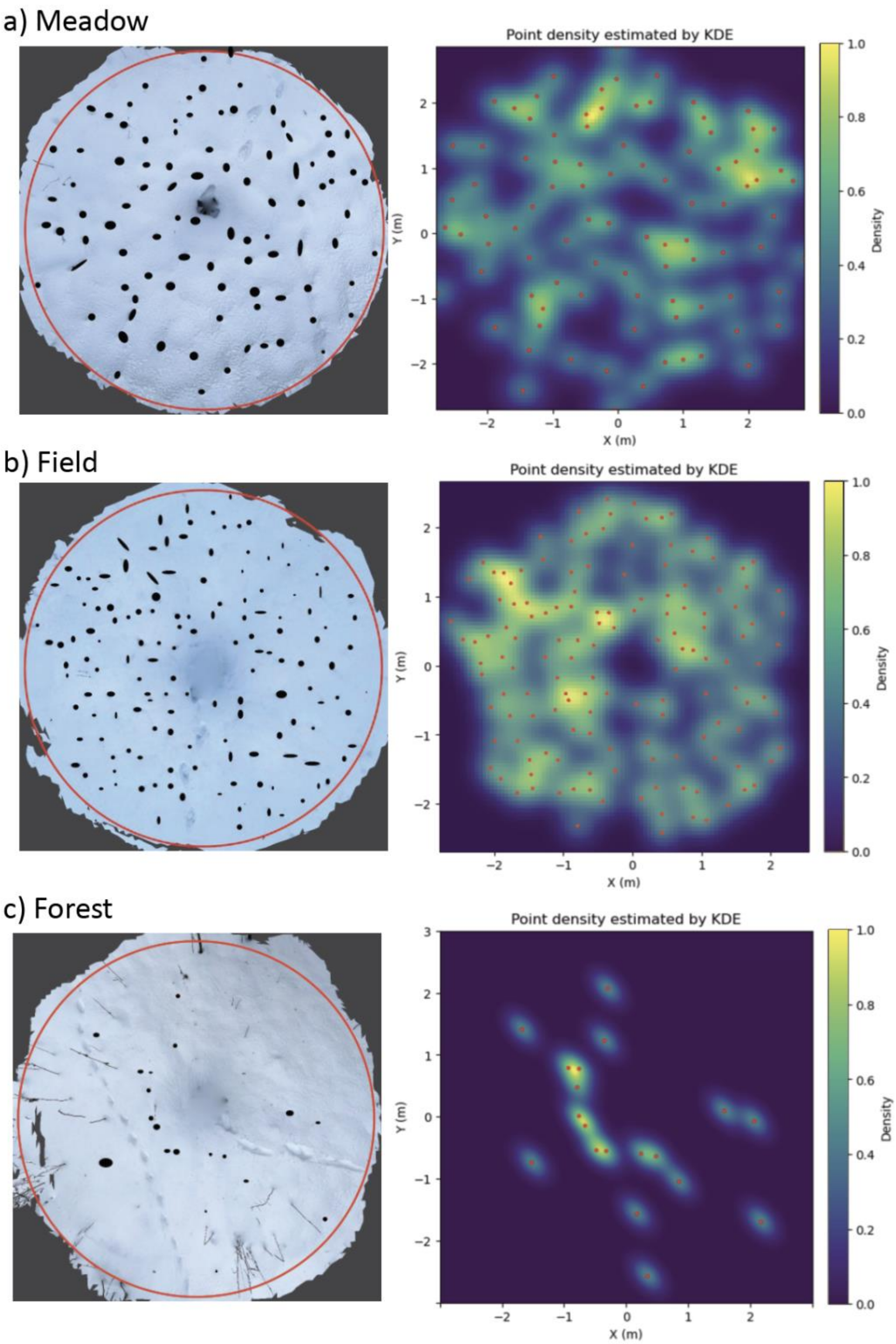

https://doi.org/10.5194/egusphere-2026-3873
Preprint. Discussion started: 14 August 2026

Fig. 4 Spatial distribution of mapped percolation funnels and corresponding kernel density estimation (KDE) maps for the floodplain meadow (a), watershed field (b), and birch forest (c) sites. Left panels show the detected funnels within the analysis circle (3 m radius), and right panels show the corresponding centroid density fields.

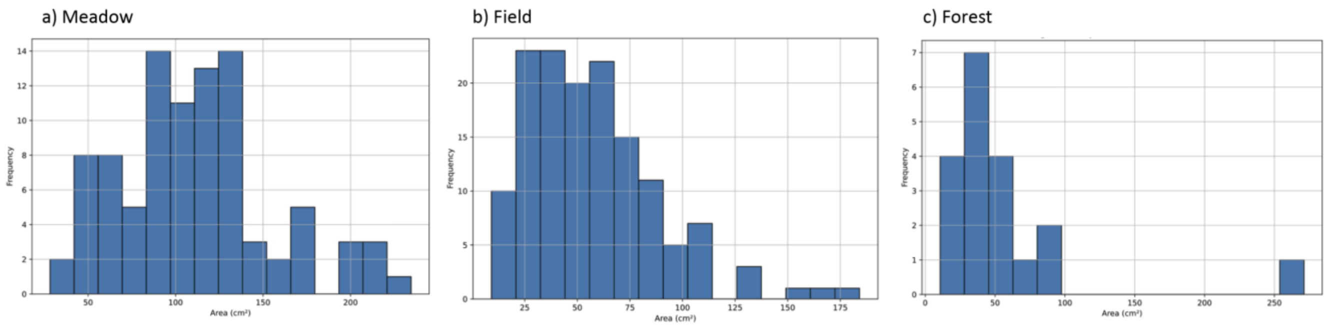

Fig. 5 Frequency distributions of percolation depression area (cm²) derived from photogrammetric analysis for the floodplain meadow(a), watershed field (b), and birch forest (c).

Meadow

At the floodplain meadow, percolation features were strongly associated with tussock microtopography. Visual observations indicated that funnels and columns developed mainly in depressions between tussocks, whereas they were not observed near tussock tops. This suggests that small-scale surface relief helped concentrate liquid water in inter-tussock hollows, where it could enter the snowpack preferentially.

The meadow exhibited a moderate spatial density of percolation features with 92 mapped percolation features (Figs. 4a and 5a). Their areas ranged from 28 to 235 cm², with a mean of 110 cm², indicating relatively large and well-developed funnels compared with the other sites. These features covered 3.6% of the surveyed surface, the highest relative coverage among the three flat sites. The mean nearest-neighbor distance was 38 cm, showing that the features were relatively frequent but not densely clustered. Most funnels fell within an intermediate size range, with the area distribution concentrated around 80–140 cm². Only few exceeded 200 cm². Ripley's L-function showed that the meadow features were generally less clustered than expected under complete spatial randomness (CSR), with the observed curve lying below the CSR expectation across most spatial scales. This indicates a tendency toward a more regular or evenly spaced arrangement of infiltration points. Taken together, the meadow was characterized by relatively large, abundant, and fairly evenly distributed percolation features, likely controlled by the repeated spacing of inter-tussock depressions. Although the Scaniverse-derived topographic data were not accurate enough to test this relationship statistically, future surveys using professional LiDAR could help quantify the link between tussock microtopography and percolation-column development.

Field

The watershed field showed a different pattern: percolation was widespread, but individual features were generally smaller than in the meadow. Because this site had the most homogeneous surface and vegetation cover, liquid water was less strongly concentrated by microtopographic depressions. As a result, water entry points were uniformly distributed across the snow

https://doi.org/10.5194/egusphere-2026-3873
Preprint. Discussion started: 14 August 2026

surface, forming numerous small funnels rather than fewer large, well-developed features. This pattern suggests that, in the absence of pronounced tussock relief, preferential infiltration still occurred but was organized at a finer spatial scale, likely controlled by small variations in crust strength, snow texture, and local wetting conditions.

This site had the greatest number of mapped percolation features, with 142 objects identified (Figs. 4b and 5b). Funnel areas ranged from 10 to 184 cm², with a mean of 57 cm². Although the features were on average nearly two times smaller than those in the meadow, their high number resulted in a total surface coverage of 2.8%. The mean nearest-neighbor distance was 28 cm, the shortest among all sites, indicating closely spaced infiltration points. The area distribution shows that most funnels were small to medium-sized, mainly between 20 and 80 cm², while larger features were rare and only a few exceeded 100–150 cm². Ripley's L-function was broadly consistent with CSR, suggesting no strong tendency toward either clustering or regular spacing. Overall, the watershed field supported numerous, relatively small percolation features that were broadly distributed across the site, consistent with more spatially uniform preferential infiltration.

Forest

The birch forest showed the strongest suppression and localization of percolation features. Despite having microtopographic variability comparable to the meadow, only a few columns developed, and these were mainly located in a gap between two adjacent birch trees. In contrast, no percolation features were observed in areas directly influenced by tree canopies. This suggests that forest vegetation and canopy-related surface roughness appeared to limit and localize where water entered the snowpack.

The forest snow surface also showed greater roughness at the 0.5–2 cm scale than the other sites. This roughness likely resulted from canopy interception of liquid precipitation and subsequent unloading of large droplets onto the snow surface, creating microscale heterogeneity. Such roughness may have disrupted lateral water movement along the surface crust and limited the formation of larger, more continuous percolation features.

Only 19 percolation features were mapped at the forest site (Figs. 4c and 5c), making it the sparsest of the three flat sites. Relative surface coverage was only 0.4%, and the mean nearest-neighbor distance was 54 cm, much larger than at the open sites. Feature areas ranged from 11 to 271 cm², with a mean of 55 cm² and high variability. Most funnels were small, generally below 60 cm², while the presence of one very large feature produced a strongly right-skewed size distribution. Ripley's L-function lay above the CSR expectation, indicating clustering rather than regular spacing. Together, these observations show that the birch forest produced sparse, clustered, and highly variable percolation features, in contrast to the more widespread patterns observed at the open sites.

Slope

At the slope site, preferential flow was expressed in a fundamentally different way. Instead of forming discrete vertical percolation columns, liquid water was routed into elongated, downslope flow paths. This indicates that surface gradient changed the dominant geometry of preferential flow from localized vertical infiltration to laterally connected drainage.

https://doi.org/10.5194/egusphere-2026-3873
Preprint. Discussion started: 14 August 2026

Three linear features were mapped at the slope site, with a combined length of 37 m. Individual lengths were variable, with a mean of 12.3 m, a median of 16 m, and a standard deviation of 7 m. The features had a mean orientation of 93°, showing strong alignment with the local slope. Their mean centroid distance to the plot center was 1.4 m, indicating that the flow paths extended broadly across the surveyed area. Unlike the flat sites, where preferential flow appeared mainly as funnels and vertical columns, the slope promoted continuous, channelized flow. Snow-pit observations suggest that these pathways were associated with stratigraphic contrasts and crust interfaces, which facilitated lateral redistribution of water downslope. Thus, at the slope site, preferential-flow geometry was controlled jointly by surface gradient and internal snow layering.

3.4 Morphology and volumetric properties of preferential-flow structures

In addition to the spatial distribution of percolation features, we analyzed the morphology and volumetric properties of individual percolation columns at the meadow and field sites. At both sites, snow within the columns was consistently denser and stored more SWE than the surrounding snow occupying the same volume, indicating that the columns acted as localized zones of water accumulation, refreezing, and enhanced mass storage. However, the morphology of the columns differed between the two sites. Columns at the meadow site were generally larger and more structurally developed than those at the field site, likely because the pronounced tussock microtopography promoted lateral concentration of liquid water from adjacent raised surfaces into inter-tussock depressions.

Figure 6 illustrates the conceptual morphology of two representative percolation columns and highlights their main structural elements. In both examples, the column begins at the snow surface as a percolation funnel, which represents the main entry point for liquid water. From this funnel, water was routed downward through a narrower, vertically elongated column body, forming a preferential flow path that crossed several snow layers. The contrast between the broad surface funnel and the narrower column body suggests that liquid water was initially concentrated over a wider surface area and then focused into a confined vertical pathway within the snowpack.

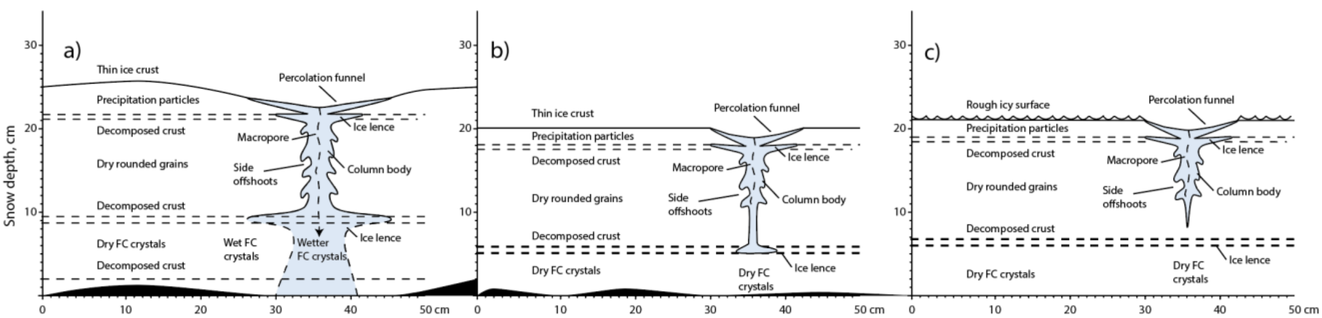

Fig. 6 Schematic representation of observed percolation-column morphology at the meadow (a), field (b) and forest (c) sites.

https://doi.org/10.5194/egusphere-2026-3873
Preprint. Discussion started: 14 August 2026

The internal structure of the columns indicates that flow was controlled by snow stratigraphy. Both columns penetrated a sequence of distinct layers, including precipitation particles near the surface, a decomposed crust, dry rounded grains, dry faceted crystals, and wet faceted crystals. These layers differed in grain type, density, and hydraulic properties, creating vertical contrasts that likely influenced both downward transmission and lateral redistribution of water. As a result, preferential flow did not develop in a homogeneous medium, but rather evolved through interaction with a layered snowpack.

Several structural features show that the flow pathways were complex. Ice lenses occurred adjacent to the main column body, particularly near crusts and stratigraphic interfaces. These features likely formed where percolating water encountered textural or permeability contrasts, spread laterally, and then refroze. Macropores in the upper and central parts of the columns may have acted as larger drain that enhanced rapid downward water transfer. In addition, lateral offshoots extended from the main column body, especially at mid-depth, indicating that part of the flow diverged sideways along capillary barriers or textural boundaries before refreezing or reconnecting with the main preferential pathway (Fig. 6).

Despite these common elements, the two columns differed in geometry and degree of development. At the meadow (Fig. 6a), the surface funnel was broader and the column body was wider and more irregular. Lateral offshoots were more pronounced, and the lower part of the column expanded into a broader wetted zone associated with faceted crystals. This morphology suggests a more complex and strongly developed preferential-flow structure, with substantial interaction between vertical flow in the main column and lateral redistribution into adjacent layers. The lower part of the column also appears to connect more directly with deeper stratigraphic interfaces, suggesting greater penetration and a stronger potential for water transfer toward the lower snowpack and ground surface.

At the field and forest (Fig. 6b, c), the columns were more compact and vertically constrained. The surface funnels were smaller and shallower, while the body remained relatively narrow throughout its depth. Although macropores and lateral offshoots were still present, they were less developed than at the field, and the surrounding wetted zone was more limited. This indicates a simpler and more localized preferential-flow path, in which water remained more tightly focused within the main column and had a weaker influence on adjacent snow layers.

Overall, these observations show that percolation columns are vertically connected but structurally heterogeneous features composed of a surface funnel, main column body, macropores, lateral offshoots, and associated ice lenses. Their morphology reflects the combined influence of surface water concentration, snow stratigraphy, and hydraulic contrasts within the snowpack. The comparison between the sites further suggests that local microtopography affects not only the spatial distribution of percolation columns, but also their size, connectivity, and degree of internal development. These structural

https://doi.org/10.5194/egusphere-2026-3873
Preprint. Discussion started: 14 August 2026

differences were also reflected in the volumetric properties of the columns. To quantify this effect, we compared the mass, density, and SWE of column snow with surrounding snow occupying the same volume at the meadow and field sites.

In contrast to the vertical percolation columns observed at the meadow and field sites, the slope site showed a more linear and stepwise flow structure (Fig. 7). In the upper part of the flow path, water appeared to move mainly along the surface ice crust. Further downslope, accumulated water locally penetrated through the crust and moved downward through the snowpack. When this vertical flow reached another low-permeability crust or stratigraphic interface, it was redirected laterally again along the same downslope thalweg. This repeated sequence of lateral flow, vertical penetration, and renewed lateral redistribution formed a ladder-like internal structure within the snowpack. The linear features were typically 10–30 cm wide and became wider toward the lower part of the slope.

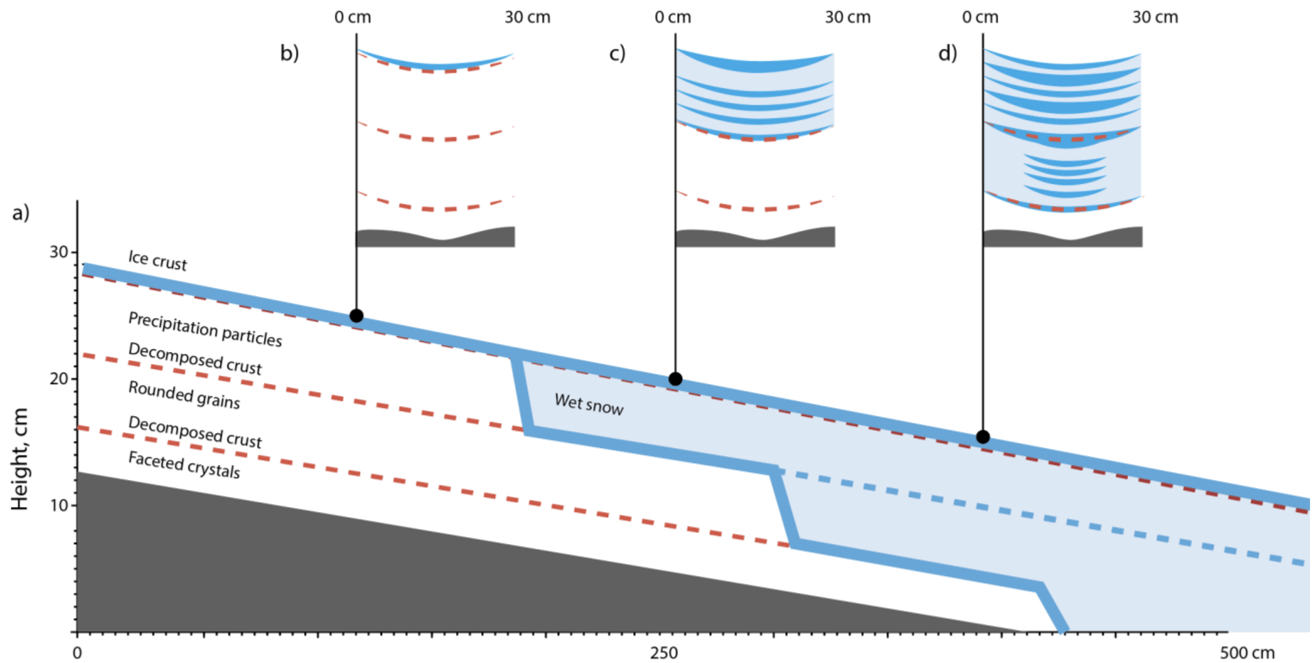

Fig. 7 Schematic representation of slope-aligned preferential flow during the ROS event. Liquid water was initially routed downslope along a low-permeability surface crust and microscale thalwegs (a, b). Local penetration through crust weak points, followed by renewed lateral flow along lower stratigraphic interfaces (c, d), produced ladder-like linear flow structures that widened downslope.

The volumetric measurements confirmed that percolation columns stored more mass and water than the same volume of undisturbed snow. At the meadow site, snow within the columns had a mass of 223 g, a density of 292 kg m^{-3}, and an SWE of 55.5 mm. In comparison, the same volume of surrounding snow had a mass of 163.4 g, a density of 214 kg m^{-3}, and an SWE of 40.7 mm. Thus, the columns contained 59.6 g more mass, were 78 kg m^{-3} denser, and stored 14.8 mm more SWE than the adjacent snow. In relative terms, column snow contained 36.4% more mass.

https://doi.org/10.5194/egusphere-2026-3873
Preprint. Discussion started: 14 August 2026

A similar pattern was observed at the field site. Snow within the columns had a mass of 210 g, a density of 303 kg m⁻³, and an SWE of 36.4 mm, compared with 148.2 g, 214 kg m⁻³, and 25.7 mm in the surrounding snow. This corresponds to increases of 61.8 g in mass, 89 kg m⁻³ in density, and 10.7 mm in SWE, or 41.6% more mass within the columns.

Overall, these results show that percolation columns acted as localized zones of water accumulation and refreezing, with substantially higher density and SWE than the surrounding snow. Although the columns occupied only 3.6% of the surface area in the meadow and 2.8% in the field, they accounted for approximately 4–5% of the total SWE. This indicates a clear concentration of mass within the columns relative to the surrounding snowpack. The relative enrichment was slightly greater at the field site, suggesting either more efficient local water retention or a stronger contrast between the columns and adjacent snow.

4. Discussion

4.1 Formation mechanism and local controls

The observations suggest a sequence in which liquid precipitation first froze on contact with the cold snow surface, forming a thin surface crust. Continued water input then promoted short-distance surface redistribution and ponding in depressions. Water entered the snowpack preferentially through weak points in the crust and was then routed vertically or laterally depending on local stratigraphy, microtopography, vegetation, and slope. Subsequent cooling refroze these pathways, preserving the columns, ice lenses, and linear drainage structures observed during field measurements.

The results show that ROS-induced percolation was strongly influenced by local surface conditions, even though all sites experienced the same regional meteorological event and had broadly comparable, but not identical, pre-event snow stratigraphy. Microtopography, vegetation, canopy effects, slope, and internal layering can therefore influence how and where liquid water enters and moves through the snowpack (Sturm and Holmgren, 1994; Liston, 2004; Komarov et al., 2018; Komarov, 2021; Komarov and Sturm, 2023). Similar microtopographic controls on water movement have been reported in tundra and hillslope systems, where inter-tussock areas or variable saturated zones can influence flow pathways (Quinton et al., 2004; Judd and Kling, 2002). Although these studies focus on soil and hillslope hydrology rather than snowpack percolation, they support the broader interpretation that small-scale surface structure can organize water movement.

A key implication is that the post-ROS snowpack cannot always be represented as a set of horizontally uniform layers. Percolation columns, ice lenses, lateral offshoots, and linear drainage pathways create strong vertical and lateral inhomogeneity. These structures concentrate water and mass in localized zones, influence refreezing and meltwater storage, and may affect the timing and pathways of water release from the snowpack (Colbeck, 1972; Marsh and Woo, 1984; Wever et al., 2014; Würzer et al., 2016). Although not measured directly here, they may also create small-scale contrasts in insulation, soil heat exchange, and water delivery to the ground, which are relevant for vegetation, soil biota, and freeze–thaw dynamics (Zhang, 2005; Rixen et al., 2022).

4.2 Methodological limitations

The use of Scaniverse provided a practical way to document the spatial organization of percolation features at the plot scale. It helped bridge the gap between point-scale snow-pit observations and broader spatial patterns by allowing rapid mapping of funnel size, density, spacing, and arrangement. This was particularly useful because many of the observed features occurred at scales that are difficult to capture with traditional snow-pit measurements alone.

We also carried out a simple field check of scan reliability by comparing distances between selected percolation column centers measured from the Scaniverse-derived images with corresponding in situ ruler measurements. For short distances of 10–50 cm, the differences were typically close to 1 cm, suggesting that the scans were sufficiently accurate for estimating relative spacing among nearby features. However, discrepancies increased over longer distances and for features located farther from the Scaniverse measurement point. This pattern indicates that the method is useful for comparative analysis of feature distribution, but less reliable for precise topographic measurements across larger parts of the scan.

These results are consistent with broader limitations of smartphone-based photogrammetry, whose accuracy depends on device specifications, scanning technique, illumination, surface texture, and environmental conditions (Łabędź et al., 2022; Paukkonen, 2023; Di Stefano et al., 2021; Treccani et al., 2024). In this study, the Scaniverse-derived data were therefore suitable for comparing spatial patterns among sites, but not for resolving subtle topographic controls, such as the exact relationship between tussock geometry and funnel position. Manual delineation of features also introduced operator subjectivity, and small or weakly expressed funnels may have been missed or underestimated. The photogrammetric results should therefore be interpreted mainly as comparative indicators of spatial organization rather than precise topographic measurements.

4.3 Broader use and future potential

Despite these limitations, low-cost phone-based photogrammetry has strong potential for snow and hydrology research. Its main value is accessibility: it allows rapid, repeatable field documentation using only a smartphone, making it useful in remote sites or exploratory studies where survey-grade instruments are unavailable. It can help expand observations of small-scale snowpack heterogeneity, particularly for processes such as crust breaching, preferential infiltration, percolation-column development, and surface drainage formation.

Future work should combine this approach with direct measurements of liquid-water content, snow temperature, density, SWE, and water fluxes. Repeated observations before and after ROS events would help determine how often such features form and how their geometry changes with snow type, vegetation, slope, and rain intensity. Validation with professional LiDAR or ground control points would also improve confidence in the spatial measurements.

More broadly, smartphone-based mapping could support model evaluation and remote-sensing interpretation by providing intermediate-scale information between snow pits and satellite observations. The method does not replace high-precision

https://doi.org/10.5194/egusphere-2026-3873
Preprint. Discussion started: 14 August 2026

instruments, but it offers a practical way to build larger observational datasets on ROS impacts and preferential-flow development under changing winter conditions.

5. Conclusion

This study demonstrates that well-defined and spatially variable percolation columns can develop in a cold, layered, predominantly fine-grained snowpack after a ROS event. The resulting structures were strongly site-dependent: the floodplain meadow was characterized by the largest average funnels and the highest relative areal coverage, the watershed field by the greatest number of smaller and closely spaced features, the birch forest by sparse and clustered features, and the slope by elongated laterally connected pathways aligned with the local gradient. These contrasts indicate that microtopography, vegetation, slope, and stratigraphy can reorganize liquid-water input at sub-meter scales.

At the meadow and field sites, percolation columns contained denser snow and higher SWE than the surrounding snow, confirming that they acted as localized zones of water accumulation and refreezing. Low-cost Scaniverse mapping provided a practical way to document these patterns, although the results should be interpreted primarily as comparative indicators of spatial organization rather than precise topographic measurements. Overall, the findings highlight the need to account for small-scale preferential-flow structures in snow hydrology, ecological interpretation, modelling, and remote sensing after ROS events.

Code and data availability

The Python/Jupyter Notebook used for the spatial analysis of percolation features, together with the processed feature measurements used to generate the reported statistics, will be provided in a Zenodo public repository upon manuscript acceptance. It is currently available from https://github.com/OneTone9/Image_analysis_workflow. Weather station data and field notes are available from the author upon request.

Author contributions

AK designed the study, carried out the field measurements, processed and analyzed the data, prepared the figures, and wrote the manuscript. JS supervised and edited the manuscript and supported the research by providing funding. Both authors contributed to the final manuscript.

Competing interests

The author declares that he has no conflict of interest.

https://doi.org/10.5194/egusphere-2026-3873
Preprint. Discussion started: 14 August 2026

Acknowledgements

The author thanks colleagues and collaborators who supported the fieldwork and discussions related to this study. The author used AI-based language-editing tools for minor grammar and formatting assistance. All scientific interpretations, analyses, and final text were performed, checked and approved by the author.

Financial support

This work was supported by the Canada 150 Research Chairs program (#50296) and by funding associated with the Helmholtz Professorship of JS at the Alfred Wegener Institute, Helmholtz Centre for Polar and Marine Research.

References

1. Albert, M. R., Shultz, E. F., and Perron, F. E. (2000). Snow and firn permeability at Siple Dome, Antarctica. Annals of Glaciology, 31, 353–356. https://doi.org/10.3189/172756400781820273
2. Barnett, T. P., Adam, J. C., and Lettenmaier, D. P. (2005). Potential impacts of a warming climate on water availability in snow-dominated regions. Nature, 438, 303–309. https://doi.org/10.1038/nature04141
3. Bartsch, A., Kumpula, T., Forbes, B. C., and Stammler, F. (2010). Detection of snow surface thawing and refreezing in the Eurasian Arctic with QuikSCAT: implications for reindeer herding, Ecological Applications, 20(8), 2346–2358, https://doi.org/10.1890/09-1927.1
4. Bintanja, R., and Andry, O. (2017). Towards a rain-dominated Arctic. Nature Climate Change, 7, 263–267. https://doi.org/10.1038/nclimate3240
5. Bouchard, B., Nadeau, D. F., Domine, F., Wever, N., Michel, A., Lehning, M., and Isabelle, P.-E. (2024). Impact of intercepted and sub-canopy snow microstructure on snowpack response to rain-on-snow events under a boreal canopy. The Cryosphere, 18, 2783–2807. https://doi.org/10.5194/tc-18-2783-2024
6. Bouvet, L., Allet, N., Calonne, N., Flin, F., et al. (2025). Simulating liquid water distribution at the pore scale in snow: Water retention curves and effective transport properties. EGUsphere [preprint]. https://doi.org/10.5194/egusphere-2025-2903
7. Colbeck, S. C. (1972). A theory of water percolation in snow. Journal of Glaciology, 11(63), 369–385. https://doi.org/10.3189/S0022143000022346
8. Colbeck, S. C. (1974). The capillary effects on water percolation in homogeneous snow. Journal of Glaciology, 13(67), 85–97. https://doi.org/10.3189/S002214300002339X
9. Coléou, C., and Lesaffre, B. (1998). Irreducible water saturation in snow: Experimental results in a cold laboratory. Annals of Glaciology, 26, 64–68. https://doi.org/10.3189/1998AoG26-1-64-68

10. Di Stefano, F., Chiappini, S., Gorreja, A., Balestra, M., and Pierdicca, R. (2021). Mobile 3D scan LiDAR: A literature review. Geomatics, Natural Hazards and Risk, 12(1), 2387–2429. https://doi.org/10.1080/19475705.2021.1964617
11. Donahue, C., and Hammonds, K. (2022). Laboratory observations of preferential flow paths in snow using upward-looking polarimetric radar and hyperspectral imaging. Remote Sensing, 14(10), 2297. https://doi.org/10.3390/rs14102297
12. Fierz, C., Armstrong, R. L., Durand, Y., Etchevers, P., Greene, E., et al. (2009). The International Classification for Seasonal Snow on the Ground. IHP-VII Technical Documents in Hydrology No. 83, IACS Contribution No. 1. UNESCO-IHP, Paris.
13. Forbes, B. C., Kumpula, T., Meschtyb, N., Laptander, R., Macias-Fauria, M., Zetterberg, P., Verdonen, M., Skarin, A., Kim, K.-Y., Boisvert, L. N., Stroeve, J. C., and Bartsch, A. (2016) Sea ice, rain-on-snow and tundra reindeer nomadism in Arctic Russia, Biology Letters, 12, 20160466, https://doi.org/10.1098/rsbl.2016.0466
14. Formozov, A. N. (1990). Snow cover as an environmental factor and its importance in the life of mammals and birds of the USSR. Moscow State University Press. (In Russian).
15. Hirashima, H., Avanzi, F., and Yamaguchi, S. (2017). Liquid water infiltration into a layered snowpack: Evaluation of a 3-D water transport model with laboratory experiments. Hydrology and Earth System Sciences, 21, 5503–5515. https://doi.org/10.5194/hess-21-5503-2017
16. Hirashima, H., Yamaguchi, S., and Katsushima, T. (2014). A multi-dimensional water transport model to reproduce preferential flow in snow. Cold Regions Science and Technology, 108, 80–90. https://doi.org/10.1016/j.coldregions.2014.09.004
17. Hirashima, H., Yamaguchi, S., Sato, A., and Lehning, M. (2010). Numerical modeling of liquid water movement through layered snow based on new measurements of the water retention curve. Cold Regions Science and Technology, 64(2), 94–103. https://doi.org/10.1016/j.coldregions.2010.09.003
18. Hock, R. (2005). Glacier melt: A review of processes and their modelling. Progress in Physical Geography, 29, 362–391. https://doi.org/10.1191/0309133305pp453ra
19. Judd, K. E., and Kling, G. W. (2002). Production and export of dissolved C in arctic tundra mesocosms: The roles of vegetation and water flow. Biogeochemistry, 60, 213–234. https://doi.org/10.1023/A:1020371412061
20. Katsushima, T., Kumakura, T., and Takeuchi, Y. (2009). A multiple snow layer model including a parameterization of vertical water channel process in snowpack. Cold Regions Science and Technology, 59(2–3), 143–151. https://doi.org/10.1016/j.coldregions.2009.09.002
21. Katsushima, T., Yamaguchi, S., Kumakura, T., and Sato, A. (2013). Experimental analysis of preferential flow in dry snowpack. Cold Regions Science and Technology, 85, 206–216. https://doi.org/10.1016/j.coldregions.2012.09.012
22. Kokhanovsky, A., Lamare, M., Di Mauro, B., Picard, G., Arnaud, L., Dumont, M., Tuzet, F., Brockmann, C., and Box, J. E. (2018). On the reflectance spectroscopy of snow. The Cryosphere, 12, 2371–2382. https://doi.org/10.5194/tc-12-2371-2018

https://doi.org/10.5194/egusphere-2026-3873
Preprint. Discussion started: 14 August 2026

23. Komarov, A. Y. (2021a). Snow cover stratigraphy in the northeast of Moscow region. Ice and Snow, 61(3), 391–403. https://doi.org/10.31857/S2076673421030096
24. Komarov, A. Y. (2021b). The influence of vegetation cover and microrelief on snow stratigraphy in the Moscow region. Moscow University Bulletin. Series 5. Geography, 87–98. (In Russian).
25. Komarov, A. Y., and Sturm, M. (2023). Local variability of a taiga snow cover due to vegetation and microtopography. Arctic, Antarctic, and Alpine Research, 55(1), 2170086. https://doi.org/10.1080/15230430.2023.2170086
26. Komarov, A. Y., Seliverstov, Y. G., Grebennikov, P. B., and Sokratov, S. A. (2018). Spatio-temporal heterogeneity of the snow cover from data of the penetrometer SnowMicroPen. Ice and Snow, 58(4), 473–485. https://doi.org/10.15356/2076-6734-2018-4-473-485
27. Komarov, A. Y., Seliverstov, Y. G., Grebennikov, P. B., & Sokratov, S. A. (2019). Spatial variability of snow water equivalent–the case study from the research site in Khibiny Mountains, Russia. Journal of Hydrology and Hydromechanics, 67(1), 110-112. https://doi.org/10.2478/johh-2018-0016
28. Komarov, A., Turchaninova, A., Seliverstov, Y., Sokratov, S., and Stroeve, J. (2025). The impact of urban heat island on snow properties and stratigraphy in the Moscow region. Urban Climate, 62, 102545. https://doi.org/10.1016/j.uclim.2025.102545
29. Łabędź, P., Skabek, K., Ozimek, P., Rola, D., Ozimek, A., and Ostrowska, K. (2022). Accuracy verification of surface models of architectural objects from the iPad LiDAR in the context of photogrammetry methods. Sensors, 22(21), 8504. https://doi.org/10.3390/s22218504
30. Lehning, M., Völksch, I., Gustafsson, D., Nguyen, T. A., Stähli, M., and Zappa, M. (2006). ALPINE3D: A detailed model of mountain surface processes and its application to snow hydrology. Hydrological Processes, 20(10), 2111–2128. https://doi.org/10.1002/hyp.6204
31. Leroux, N. R., and Pomeroy, J. W. (2017). Modelling capillary hysteresis effects on preferential flow through melting and cold layered snowpacks. Advances in Water Resources, 107, 250–264. https://doi.org/10.1016/j.advwatres.2017.06.024
32. Liston, G. E. (2004). Representing subgrid snow cover heterogeneities in regional and global models. Journal of Climate, 17(6), 1381–1397. https://doi.org/10.1175/1520-0442(2004)017<1381:RSSCHI>2.0.CO;2
33. Lombardo, M., Fees, A., Kaestner, A., van Herwijnen, A., Schweizer, J., and Lehmann, P. (2025). Quantification of capillary rise dynamics in snow using neutron radiography. The Cryosphere, 19, 4437–4458. https://doi.org/10.5194/tc-19-4437-2025
34. Madore, J. B., Fierz, C., and Langlois, A. (2022). Investigation into percolation and liquid water content in a multi-layered snow model for wet snow instabilities in Glacier National Park, Canada. Frontiers in Earth Science, 10, 898980. https://doi.org/10.3389/feart.2022.898980

https://doi.org/10.5194/egusphere-2026-3873
Preprint. Discussion started: 14 August 2026

35. Marsh, P., and Woo, M. K. (1984). Wetting front advance and freezing of meltwater within a snow cover: 1. Observations in the Canadian Arctic. Water Resources Research, 20(12), 1853–1864. https://doi.org/10.1029/WR020i012p01853
36. Merkouriadi, I., Lemmetyinen, J., Liston, G. E., and Pulliainen, J. (2021). Solving challenges of assimilating microwave remote sensing signatures with a physical model to estimate snow water equivalent. Water Resources Research, 57, e2021WR030119. https://doi.org/10.1029/2021WR030119
37. Miller, S. H., Hashemian, A., Gillihan, R., and Helms, E. (2022). A comparison of mobile phone LiDAR capture and established ground-based 3D scanning methodologies. SAE Technical Paper 2022-01-0832. https://doi.org/10.4271/2022-01-0832
38. Montpetit, B., Royer, A., Roy, A., Langlois, A., and Derksen, C. (2013). Snow microwave emission modeling of ice lenses within a snowpack using the Microwave Emission Model for Layered Snowpacks. IEEE Transactions on Geoscience and Remote Sensing, 51(9), 4705–4717. https://doi.org/10.1109/TGRS.2013.2250509
39. Mott, R., Schlögl, S., Dirks, L., and Lehning, M. (2017). Impact of extreme land surface heterogeneity on micrometeorology over spring snow cover. Journal of Hydrometeorology, 18(10), 2705–2722. https://doi.org/10.1175/JHM-D-17-0074.1
40. Moure, A., Jones, N., Pawlak, J., Meyer, C., and Fu, X. (2023). A thermodynamic nonequilibrium model for preferential infiltration and refreezing of melt in snow. Water Resources Research, 59(5), e2022WR034035. https://doi.org/10.1029/2022WR034035
41. Nolin, A. W., and Dozier, J. (2000). A hyperspectral method for remotely sensing the grain size of snow. Remote Sensing of Environment, 74(2), 207–216. https://doi.org/10.1016/S0034-4257(00)00111-5
42. Paukkonen, N. (2023). Towards a mobile 3D documentation solution: Video-based photogrammetry and iPhone 12 Pro as fieldwork documentation tools. Journal of Computer Applications in Archaeology, 6(1), 143–154. https://doi.org/10.5334/jcaa.135
43. Pinzner, A., Sturm, M., Delamere, J. S., and Mahoney, A. R. (2024). An examination of water-related melt processes in Arctic snow on tundra and sea ice. Water Resources Research, 60(1), e2022WR033440. https://doi.org/10.1029/2022WR033440
44. Pomeroy, J. W., and Brun, E. (2001). Physical properties of snow. In Snow Ecology: An Interdisciplinary Examination of Snow-Covered Ecosystems, 45–118.
45. Putkonen, J., and Roe, G. J. (2003). Rain-on-snow events impact soil temperatures and affect ungulate survival. Geophysical Research Letters, 30(4). https://doi.org/10.1029/2002GL016326
46. Quinton, W. L., Carey, S. K., and Goeller, N. T. (2004). Snowmelt runoff from northern alpine tundra hillslopes: Major processes and methods of simulation. Hydrology and Earth System Sciences, 8, 877–890. https://doi.org/10.5194/hess-8-877-2004

https://doi.org/10.5194/egusphere-2026-3873
Preprint. Discussion started: 14 August 2026

47. Rixen, C., Høye, T. T., Macek, P., Aerts, R., Alatalo, J. M., Anderson, J. T., et al. (2022). Winters are changing: Snow effects on Arctic and alpine tundra ecosystems. Arctic Science, 8(3), 572–608. https://doi.org/10.1139/as-2020-0058
48. Serreze, M. C., Gustafson, J., Barrett, A. P., Druckenmiller, M. L., Fox, S., Voveris, J., Stroeve, J., Sheffield, B., Forbes, B. C., Rasmus, S., Laptander, R., Brook, M., Brubaker, M., Temte, J., McCrystall, M. R., and Bartsch, A. (2021). Arctic rain on snow events: bridging observations to understand environmental and livelihood impacts, Environmental Research Letters, 16(10), 105009, https://doi.org/10.1088/1748-9326/ac269b
49. Sokratov, S. A., Komarov, A. Y., Vasil'chuk, Y. K., et al. (2024). Spatial-temporal variability of the δ18O values and the snow cover structure on the territory of the Meteorological Observatory of Moscow State University. Water Resources, 51(Suppl. 1), S89–S99. https://doi.org/10.1134/S0097807824701367
50. Stroeve, J., Nandan, V., Willatt, R., Dadic, R., Rotosky, P., Gallagher, M., et al. (2022). Rain-on-snow (ROS) understudied in sea ice remote sensing: A multi-sensor analysis of ROS during MOSAiC. The Cryosphere, 16, 4223–4250. https://doi.org/10.5194/tc-16-4223-2022
51. Sturm, M. (1992). Snow distribution and heat flow in the taiga. Arctic and Alpine Research, 24(2), 145–152. https://doi.org/10.1080/00040851.1992.12002939
52. Sturm, M., and Holmgren, J. (1994). Effects of microtopography on texture, temperature and heat flow in Arctic and sub-Arctic snow. Annals of Glaciology, 19, 63–68. https://doi.org/10.3189/1994AoG19-1-63-68
53. Treccani, D., Adami, A., and Fregonese, L. (2024). Assessing the effectiveness of LiDAR-based apps on Apple devices to survey indoor and outdoor medium-sized areas. The International Archives of the Photogrammetry, Remote Sensing and Spatial Information Sciences, 48, 431–438. https://doi.org/10.5194/isprs-archives-XLVIII-2-W8-2024-431-2024
54. Webb, R. W., Musselman, K. N., Ciafone, S., Hale, K. E., and Molotch, N. P. (2022). Extending the vadose zone: Characterizing the role of snow for liquid water storage and transmission in streamflow generation. Hydrological Processes, 36(3), e14541. https://doi.org/10.1002/hyp.14541
55. Wever, N., Fierz, C., Mitterer, C., Hirashima, H., and Lehning, M. (2014). Solving Richards equation for snow improves snowpack meltwater runoff estimations in a detailed multi-layer snowpack model. The Cryosphere, 8(1), 257–274. https://doi.org/10.5194/tc-8-257-2014
56. Wiesmann, A., and Mätzler, C. (1999). Microwave emission model of layered snowpacks. Remote Sensing of Environment, 70(3), 307–316. https://doi.org/10.1016/S0034-4257(99)00046-2
57. Würzer, S., Jonas, T., Wever, N., and Lehning, M. (2016). Influence of initial snowpack properties on runoff formation during rain-on-snow events. Journal of Hydrometeorology, 17(6), 1801–1815. https://doi.org/10.1175/JHM-D-15-0181.1
58. Würzer, S., Wever, N., Juras, R., Lehning, M., and Jonas, T. (2017). Modelling liquid water transport in snow under rain-on-snow conditions: Considering preferential flow. Hydrology and Earth System Sciences, 21(3), 1741–1756. https://doi.org/10.5194/hess-21-1741-2017

https://doi.org/10.5194/egusphere-2026-3873
Preprint. Discussion started: 14 August 2026

59. Yamaguchi, S., Katsushima, T., Sato, A., and Kumakura, T. (2012). Dependence of the water retention curve of snow on snow characteristics. Annals of Glaciology, 53(61), 6–12. https://doi.org/10.3189/2012AoG61A001
60. Zhang, T. (2005). Influence of seasonal snow cover on ground thermal regime. Reviews of Geophysics, 43, RG4002. https://doi.org/10.1029/2004RG000157
61. Zhu, J., Tan, S., Tsang, L., Kang, D.-H., and Kim, E. J. (2021). Snow water equivalent retrieval using active and passive microwave observations. Water Resources Research, 57, e2020WR027563. https://doi.org/10.1029/2020WR027563